Cryo-EM structure of the human G-protein coupled receptor 1 (GPR1) – Gi protein complex bound to the chemerin C-terminal nonapeptide

Aijun Liu[1,5], Yezhou Liu[1,3,5], Geng Chen[1], Wenping Lyu[2], Junlin Wang[1], Qiwen Liao[1], Fang Ye[1], Lizhe Zhu[2], Yang Du[1], Richard D. Ye[1,4,*]

[1]Kobilka Institute of Innovative Drug Discovery, and [2]Warshel Institute for Computational Biology, School of Medicine, The Chinese University of Hong Kong, Shenzhen, Guangdong, 518172, P.R. China; [3]Shenzhen Bay Laboratory, Shenzhen, Guangdong, 518055, P.R. China; [4]The Chinese University of Hong Kong, Shenzhen Futian Biomedical Innovation R&D Center, Shenzhen, Guangdong 518048, P.R. China

[5]These authors contributed equally to this work.

[*]Corresponding author: Prof. Richard D. Ye (richardye@cuhk.edu.cn)

ABSTRACT

Chemerin is a chemoattractant and adipokine protein that acts on G protein-coupled receptors including chemokine-like receptor 1 (CMKLR1), G-protein coupled receptor 1 (GPR1) and C-C chemokine receptor-like 2 (CCRL2), mainly through its C-terminal peptide containing the sequence YFPGQFAFS (C-terminal nonapeptide or C9). Previous studies suggest that the three receptors respond to chemerin and C9 differently, with activation of the Gi signaling pathway through CMKLR1 but not GPR1 and CCRL2. Recently we reported a cryo-EM structure of human CMKLR1 in complex with Gi proteins and the C9 peptide. To identify structural differences among these receptors in ligand binding and Gi protein signaling, here we report a high-resolution cryo-EM structure of human GPR1-Gi complex bound to C9. Our structural and functional results show that GPR1 is able to respond to the C9 peptide with activation of the Gi signaling pathway and forms complex with Gi protein. Similar to the CMKLR1-C9 structure, C9 adopts a C-terminus-in and “S-shape” pose in the binding pocket. C9 is stabilized through hydrophobic interactions involving its Y1, F2, Q5, F6 and F8, and polar interactions between its P3, G4, Q5, F6, F8, S9 and residues lining the GPR1 binding pocket. An analysis of the GPR1-Gi protein interface found high similarities to the CMKLR1-Gi complex, and site-directed mutagenesis with functional verifications support GPR1 as a Gi-coupling receptors. These findings provide a structural basis of ligand recognition and Gi protein coupling by GPR1, and may help to understand the respective functions of the three chemerin receptors.

Keywords: GPCRs, chemerin, G proteins, cryo-EM

MAIN TEXT

Introduction

Chemerin is a small protein encoded by the retinoic acid receptor responder 2 gene. Chemerin is mainly expressed in adipose tissue, liver, lung and skin (Bozaoglu et al., 2007; Goralski et al., 2007; Lehrke et al., 2009). The role of chemerin was initially identified as a chemoattractant of inflammatory cells following its discovery in psoriasis (Kennedy & Davenport, 2018). Chemerin was subsequently found to act as an adipokine (Bozaoglu et al., 2007; Goralski et al., 2019; Goralski et al., 2007; Helfer & Wu, 2018). Secretion of chemerin requires removal of the N-terminal signaling peptides, resulting in pro-chemerin (amino acids 21-163) with a low biological activity. Further proteolytic removal of six amino acids from the C-terminus (158-163) leads to chemerin21-157 with full bioactivity (Wittamer et al., 2003). C-terminal synthetic fragments of human chemerin, including chemerin149-157 (C9), chemerin145-157 (C13) and chemerin138-157 (C20), show comparable biological activity to chemerin21-157 (Meder et al., 2003; Zabel, Allen, et al., 2005; Zabel, Silverio, et al., 2005).

To date, 3 chemerin receptors have been identified, namely chemokine-like receptor 1 (CMKLR1), G protein-coupled receptor 1 (GPR1) and C-C chemokine receptor-like 2 (CCRL2) (Barnea et al., 2008; Zabel et al., 2008). CMKLR1 responds to chemerin and the C9 peptide with activation of the G protein (Gi) pathway and the β-arrestin pathway. In contrast, CCRL2 binds chemerin but does not mediate its transmembrane signaling (Kennedy & Davenport, 2018). The biological functions of GPR1 as a chemerin receptor remains unclear. GPR1 was originally identified as an orphan receptor (Marchese et al., 1994). It was subsequently found as a chemerin receptor but published studies of its pharmacological properties vary widely. Using a reporter assay (TANGO) for measurement of β-arrestin activation, Barnea and collegues found that GPR1 activation is biased towards the β-arrestin pathway when compared with CMKLR1 (Barnea et al., 2008). Another study showed that both CMKLR1 and GPR1 could activate the β-arrestin pathway but the amplitude of the CMKLR1-mediated signaling was larger (De Henau et al., 2016). In terms of G protein activation, published studies showed downstream activities of RhoA/ROCK, $G\alpha_{q/11}$ and $G\alpha_{i/o}$, but it was not clear which one is the dominant G protein for

functional coupling (Rourke et al., 2015). Other studies have shown that human GPR1 was involved in human immunodeficiency virus replication (Samson et al., 1998; Shimizu et al., 2009; Tokizawa et al., 2000), in glucose homeostasis, cardiovascular diseases, steroid hormone synthesis and reproductive biology (Caulfield et al., 2003; Ernst & Sinal, 2010; Karagiannis et al., 2013; Kennedy & Davenport, 2018; Neves et al., 2018; Rourke et al., 2014), suggesting that the downstream signaling network of GPR1 may be diverse.

GPR1 and CMKLR1 share high sequence homology, yet their respective functions elicited by chemerin may be different. CMKLR1 is often considered a balanced receptor mediating all biological functions of chemerin. In a recent study, we reported the cryo-EM structure of CMKLR1-Gi complex bound to the C9 peptide of chemerin (Wang et al., 2023) that illustrates a clearly defined binding pocket for the C-terminal peptide of chemerin as well as an interface for Gi protein interaction. For GPR1, studies support the ligand-induced β-arrestin recruitment, yet current findings on the activation of G protein signaling by GPR1 are inconsistent and controversial (De Henau et al., 2016; Kennedy & Davenport, 2018). Given the discrepancies among current understandings of GPR1 downstream signaling pathways, it is important to understand how chemerin binds to GPR1 and whether the binding event can be translated into G protein activation. To this end, we have determined the cryo-EM structure of GPR1 bound to C9, in complex with heterotrimeric Gi proteins. Our results demonstrated the structural basis for GPR1-dependent Gi protein activation.

Methods

Expression vector design

Human GPR1 was cloned into a pFastBac vector (Invitrogen, Carlsbad, CA, USA) for protein expression and purification. Specifically, the coding sequence of human GPR1 was fused with an N-terminal HA signal peptide followed by a FLAG tag, a human rhinovirus 14 3C (HRV-3C) protease cleavage site (LEVLFQGP) and the thermostabilized apocytochrome b(562)RIL (BRIL) fusion protein (Chun et al., 2012). Human dominant negative Gαi1 (DNGαi1), generated with the G203A and A326S substitution, was cloned into a pFastBac vector. N-terminal 6×His-tagged Gβ1 and Gγ2 were cloned into a pFastBac-Dual vector. scFv16 was fused with a N-terminal GP67 signal peptide and a C-terminal 8× His tag, and the coding sequence was then cloned into a pFastBac vector.

For functional assays, the full-length human GPR1 cDNA were cloned into pcDNA3.1(+) vector (Invitrogen) with an N-terminal FLAG tag. Point mutations were introduced using homologous recombination. Two fragments of GPR1 separated at mutated positions were amplified using PCR and then assembled into pre-cut pcDNA3.1(+) vectors using the ClonExpress Ultra One Step Cloning Kit (Vazyme Biotech; C115). Plasmids with GPR1 mutations were confirmed by DNA sequencing (GENEWIZ).

Expression and purification of the GPR1-Gi complexes

The baculoviruses expressing GPR1, DNGαi1, Gβ1 and Gγ2 were generated and amplified using the Bac-to-Bac baculovirus expression system. The *Sf*9 cells were cultured in SIM SF Expression Medium (Sino Biological). When the cell density reached 3.5 × 10^6 cells/mL (in total 2 liters), the baculoviruses (GPR1, DNGαi1, Gβ1γ2) were co-expressed in *Sf*9 cells at a ratio of 1:4:2. After infection for 60 hrs, the cells were collected by centrifugation at 2,000 × g for 15 mins and kept frozen at −80°C before complex purification.

For the purification of C9 bound GPR1-Gi protein complexes, cell pellets from a 2L culture were resuspended in 150 mL lysis buffer (10 mM Tris pH 7.5, 1 mM EDTA, 2.5 μg/mL leupeptin and 160 μg/mL benzamidine, 4 μM C9 peptide and 1 mg/mL iodoacetamde) for 30 mins at room temperature. The lysate was centrifuged for 15 mins at 18,000 × g, and pellet was homogenized in 150 mL solubilization buffer (20 mM HEPES pH 7.5, 100 mM NaCl, 10% glycerol, 1% dodecylmaltoside (DDM), 0.1% cholesteryl hemisuccinate (CHS), 2.5 μg/mL leupeptin and 160 μg/mL benzamidine, 4 μM C9 peptide, 1 mg/mL iodoacetamde, 2 mg scFv16, 25 mU/mL apyrase) using a Dounce homogenizer. The sample was stirred for 2 hrs at 4°C and then centrifuged for 30 mins at 18,000 × g to remove the insoluble debris. The solubilized supernatant fraction was incubated with 2 mL anti-FLAG affinity resin (GenScript Biotech, Piscataway, NJ) and stirred at 4°C for 2 hrs. Then, the resin was manually loaded onto a gravity-flow column and extensively washed with the FLAG wash buffer (W1: 20 mM HEPES pH 7.5, 0.1% DDM, 0.01% CHS, 100 mM NaCl, 2 mM $CaCl_2$, 4 μM C9 peptide. W2: 20 mM HEPES pH 7.5, 0.2% lauryl maltose neopentyl glycol (LMNG), 0.02% CHS, 100 mM NaCl, 2 mM $CaCl_2$, 4 μM C9 peptide) by mixing W1 and W2 buffer in the following ratios: 5 mL:5 mL, 2 mL:8 mL, 1 mL:9 mL, 0.5 mL:9.5 mL, 0 mL:10 mL, respectively. The GPR1-Gi complexes attached to the resin were further eluted with 10 mL elution buffer (20 mM HEPES pH 7.5, 0.01% LMNG,

0.002% CHS, 100 mM NaCl, 4 μM C9 peptide, 5 mM EDTA, 0.2 mg/ml FLAG peptide). Eluted protein complexes were concentrated to 400 μL in an Amicon® Ultra-15 Centrifugal Filter Unit (Millipore, Burlington, MA) and further subjected to a size exclusion chromatography through a Superdex 200 Increase 10/300 column (GE Healthcare Life Sciences, Sweden) equipped in an AKTA FPLC system with running buffer (20 mM HEPES pH 7.5, 0.01% LMNG, 0.002% CHS, 100 mM NaCl, 4 μM C9 peptide). Eluted fractions containing GPR1-Gi complexes were re-pooled and concentrated as described above before being flash frozen in liquid nitrogen and stored at −80°C.

Expression and purification of scFv16

The antibody fragment scFv16 was expressed as a secretory protein and purified as previously described (Chen et al., 2022). Briefly, *Trichoplusia ni* Hi5 insect cells were cultured to reach a density of 3.5×10^6 cells/mL. Cells were then infected with scFv16 baculovirus at a ratio of 1:50. After 60 hrs of culture, the supernatant was collected and loaded onto a Ni-NTA resin column. The column was washed with 20 mM HEPES (pH 7.5), 500mM NaCl, and 20 mM imidazole, and then subjected to elution by 20 mM HEPES (pH 7.5), 100 mM NaCl, and 250 mM imidazole. The eluted proteins were concentrated and subjected to size-exclusion chromatography using a Superdex 200 Increase 10/300 column (GE Healthcare). Finally, the purified scFv16 protein with a monomeric peak was concentrated and flash frozen in liquid nitrogen and stored at −80 ˚C for further use.

Cryo-EM sample preparation and data collection

For cryo-EM sample preparation of the C9-GPR1-Gi-scFv16 complex, amorphous alloy film (CryoMatrix nickel titanium alloy film, R1.2/1.3, Zhenjiang Lehua Electronic Technology Co., Ltd.) was glow discharged in a Tergeo-EM plasma cleaner; 3 μL purified complex sample was loaded on the grid and blotted for 3 s with a blotting force of 0, and then flash-frozen in liquid ethane cooled by liquid nitrogen using Vitrobot Mark IV (Thermo Fisher Scientific, Waltham, MA). For data collection, cryo-EM data were collected at the Kobilka Cryo-EM Center of The Chinese University of Hong Kong, Shenzhen, on a 300 kV Titan Krios Gi3 microscope (Thermo Fisher Scientific). The raw movies were then recorded using a Gatan K3 BioQuantum Camera at the magnification of 105,000, with the pixel size of 0.83 Å. A GIF Quantum energy filter was applied to exclude inelastically scattered electrons (Gatan, USA) using a slit width of 20 eV. The movie stacks were acquired with a total exposure time of 2.5 s fragmented into 50 frames (0.05 s/frame). The defocus range were from −1.2 to −2.0 μm. The semi-automatic data acquisition was performed using SerialEM. A total of 3,609 image stacks were collected in 60 hrs.

Image processing and model building

Data processing was performed with cryoSPARC 3.3.1 (Structura Biotechnology Inc., Toronto, Canada). Patch motion correction and patch CTF estimation were firstly applied to the image stacks. 2,280,697 particles were auto-picked. 2D classification was performed, resulting in 732,629 particles selected for *ab initio* reconstruction. After 3 rounds heterogeneous refinements, a final set of 339,859 particles were exported to non-uniform refinement and local refinement, yielding a map with global resolution of 2.90 Å.

The predicted structure GPR1 on AlphaFold database was used to build the initial model of the receptor. The coordinates of Gi1 and scFv16 from GPR88 (PDB ID: 7WXZ) were applied as templates. All models were docked into the EM density map using UCSF Chimera version 1.12, followed by iterative manual building in Coot-0.9.2 and refinement in Phenix-1.18.2. The statistics of the final model were further validated by Phenix-1.18.2. Structure figures were generated by Chimera or PyMOL (Schrödinger, Inc., New York, NY). The statistics of data-collection and structure-refinement were shown in Supplementary Table 1.

Molecular modeling and molecular dynamic simulation

Protonation state of the GPR1 was assigned by the web server H++ (Anandakrishnan et al., 2012) assuming pH 7.4, and CHARMM36m (Anandakrishnan et al., 2012) force field was employed in all simulations. After energy minimization, membrane relaxation, and equilibrium simulation (Huang et al., 2017), ten independent 1-μs long production MD simulations were carried out for C9-GPR1 binding. Fifty-thousand conformations were collected in total from the assemble of trajectories. Hydrogen bonds were identified based on cutoffs for the Donor-H⋯Acceptor distance and angle. The criterion employed was angle > 120° and H⋯Acceptor distance < 2.5 Å in at least 10% of the trajectory.

G protein dissociation assay

G protein activation was tested by a NanoBiT-based G protein dissociation assay (Inoue et al., 2019). HEK293T cells were plated in a 24-well plate 24 hrs before transfection. Lipofectamine™ 3000 (Invitrogen, L3000001) transfection was performed with a mixture of 92 ng pcDNA3.1 vector encoding human GPR1 (WT/mutants) or WT human CMKLR1 for comparison, 46 ng pcDNA3.1 vector encoding Gαi1-LgBiT, 230 ng pcDNA3.1 vector encoding Gβ1 and 230 ng pcDNA3.1 vector encoding SmBiT-Gγ2 (per well in a 24-well plate), respectively. After 24 hrs of incubation, the transfected cells were collected and resuspended in HBSS containing 20 mM HEPES. The cell suspension was loaded onto a 384-well culture white plate (PerkinElmer Life Sciences, Waltham, MA) at a volume of 20 μL and loaded with 5 μL of 50 μM coelenterazine H (Yeasen Biotech, Shanghai, China). After 2 hrs of incubation at room temperature, the baseline was measured using an Envision 2105 multimode plate reader (PerkinElmer, Waltham, MA, USA). Then, C9 peptides (ChinaPeptides, Shanghai, China) were added to the cells to different concentration. The ligand-induced luminescence signals were measured 15 mins after ligand addition and divided by the initial baseline readouts. The fold changes of signals were further normalized to PBS-treated signal and the values (EC_{50}) were expressed as a function of different concentrations of C9 peptide ligand based on three independent experiments, each with triplicate measurements.

cAMP assay

Wild-type human GPR1 and its mutants, or wild-type human CMKLR1 for comparison, were transiently expressed in HeLa cells 24 hrs prior to collection. The cells were resuspended in HBSS buffer plus 5 mM HEPES, 0.1% BSA (w/v) and 0.5 mM 3-isobutyl-1-methylxanthine and loaded onto 384-well plates. Different concentrations of C9 peptide were prepared with 2.5 μM forskolin in the abovementioned buffer. The cells were stimulated by the ligands and 2.5 μM forskolin for 30 mins in a cell incubator. Intracellular cAMP levels were measured with the LANCE Ultra cAMP kit (PerkinElmer, TRF0263) following the manufacturer's

instructions. In the measurements, signals of time resolved-fluorescence resonance energy transfer (TR-FRET) were detected by an EnVision 2105 multimode plate reader (PerkinElmer). Intracellular cAMP levels were calculated according to the TR-FRET signals of the samples and cAMP standards.

β-arrestin recruitment assay

For NanoBiT-based β-arrestin recruitment assay, HEK293T cells were seeded in a 24-well plate 24 hrs before transfection. Cells are co-transfected with GPR1-WT-smBiT or CMKLR1-WT-smBiT (400 ng/well) and LgBiT-β-Arr1 or LgBiT-β-Arr2 (200 ng/well) by Lipofectamine™ 3000 (Invitrogen) for 24 hrs. Cells were collected and resuspended in HBSS buffer containing 20 mM HEPES, and then 20 μL of cell suspension was loaded onto a 384-well white plate at a concentration of $2x10^4$ cells/well. Test samples were further loaded with coelenterazine H to a final concentration of 10 μM. After 25 mins incubation at 37 °C, the samples were measured for baseline luminescence using an Envision 2105 multimode plate reader (PerkinElmer). Different concentrations of C9 peptide were added to the wells and the luminescence signals were detected for 30 mins. The signal readouts were further normalized to PBS-treated signal and the values (EC_{50}) were expressed as a function of different concentrations of C9 peptide ligand based on three independent experiments, each with triplicate measurements.

IP1 accumulation assay

Wild-type GPR1 and its mutants, and wild-type human CMKLR1 for comparison, were transiently expressed in HEK293T cells for 24 hrs. IP1 accumulation was tested using IP-One Gq HTRF kit (Cisbio). The cells were resuspended in the stimulation buffer (Cisbio) and incubated with different concentrations of C9 peptide diluted in the stimulation buffer for 30 mins at 37°C. The accumulation of IP1 was further determined following the manufacturer's protocols. Fluorescence intensities were measured on an Envision 2105 multimode plate reader (PerkinElmer). Intracellular IP1 levels were calculated according to the fluorescence signals of the samples and IP1 standards.

GPR1 expression level determination by flow cytometry

HEK293T cells were transfected with FALG-tagged WT or mutant GPR1 expression plasmids for 24 hrs at 37°C. Then the cells were harvested and washed in HBSS containing 5% BSA for three times on ice. The cells were then incubated with a FITC-labeled anti-FLAG antibody (M2; Sigma, Cat #F4049; 1:50 diluted by HBSS buffer) for 30 mins on ice and washed with HBSS. The FITC fluorescence signals demonstrating the antibody-receptor complex on the cell surface were quantified by flow cytometry (CytoFLEX, Beckman Coulter, Brea, CA). Relative expression levels of GPR1 mutants were represented according to the fluorescence signals.

Statistical analysis

The data were analyzed with Prism 9.5.0 (GraphPad, San Diego, CA). For dose-response analysis, the curves were plotted with the log[agonist] vs. response equation (three parameters) in the software. For cAMP, IP1, and G protein dissociation assays, data points were presented as the percentages (mean ± SEM) of the maximal response level for each sample, from at least three independent experiments, as indicated in figure legends. For the β-arrestin recruitment assay, data were presented as raw chemiluminescence signals (mean ± SEM) from at least

three independent experiments. The EC_{50} values were obtained from the dose-response curves. For cell surface expression, data points were presented as the percentages (mean ± SEM) of the flow cytometry fluorescence signals of WT GPR1. For statistical comparisons, Analysis of Variance (ANOVA) was performed using the one-way method. A *p* value of 0.05 or lower is considered statistically significant.

Results

GPR1 can activate Gi protein responses.

It has been long controversial about the downstream signaling events elicited by the activation of GPR1. We hence compared GPR1 and CMKLR1 by performing G protein dissociation assay, cAMP inhibition assay targeting the Gαi responses, IP1 accumulation assay targeting Gβγ downstream events and β-arrestin recruitment assays following C9 peptide stimulation. GPR1 elicited cAMP inhibition, although to a lesser extent in comparison with CMKLR1 (Fig. 1A). In NanoBiT G protein dissociation assay, C9 activated GPR1 and CMKLR1 with a similar EC_{50}, although the efficacy was lower for GPR1 (Fig. 1B). In IP1 accumulation assay, a downstream signaling event of Gβγ proteins, a lower EC_{50} with a similar amplitude was observed for GPR1 (Fig. 1C). These results indicate that GPR1 can activate G protein signaling pathways in response to agonist stimulation. We further extended our functional test to β-arrestin recruitment. Both CMKLR1 and GPR1 showed a preference in recruiting β-arrestin1 over β-arrestin2 (Fig. 1D). GPR1 experienced a significant lower efficacy of β-arrestin response, with nearly no recruitment of β-arrestin2. These findings demonstrate that the major signaling differences between GPR1 and CMKLR1 lie in the recruitment of β-arrestins rather than G protein activation, in contrast to previous reports (Barnea et al., 2008; De Henau et al., 2016; Degroot et al., 2022; Fischer et al., 2021; Rourke et al., 2015; Wittamer et al., 2003).

Cryo-EM structure of the GPR1-Gi complex.

To determine physical interactions between GPR1 and G proteins, we purified the receptor-Gi protein complex with the C9 peptide. As shown in Fig. S1, complex formation was readily observed between the C9-bound GPR1, Gi heterotrimer and the scFv16 antibody fragment, that served to stabilize the Gi protein heterotrimer (Maeda et al., 2018). The cryo-EM structure of the complex was determined to an overall resolution of 2.90 Å (Fig. 2A and B, Fig. S1 and S2). The ligand-binding pocket of GPR1 was surrounded by transmembrane (TM) helices 2, 3, 4, 6, 7 and the first, second and third extracellular loops (ECL1, ECL2 and ECL3) (Fig. 2A). The C9 peptide assumes a posture with its C terminus inserted to the binding pocket (Fig. 2 B-D). The peptide ligand takes an “S”-shape in the binding pocket, providing interactions between the ligand and the receptor residues. Specifically in this

354 structural model (Fig. 2 C-E), the N-terminal Y1 and F2 of the C9 peptide show
355 hydrophobic interactions with L186^{ECL2}, H273^{ECL3}, Y188^{ECL2} and I272$^{6.61}$[superscripts
356 indicate the Ballesteros-Weinstein numbering scheme for GPCRs (Ballesteros &
357 Weinstein, 1995)]. P3 in the peptide backbone formed polar interactions with
358 N189^{ECL2} and G4 has polar interactions formed between its backbone amide group
359 and E269$^{6.58}$. Q5 with its backbone carbonyl oxygen formed polar interaction with
360 Y96$^{2.63}$. The aromatic ring of F6 showed nonpolar interactions with F101^{ECL1} and
361 Q283$^{7.32}$, and the backbone carbonyl oxygen has polar interactions with Y93$^{2.60}$. F8
362 with its aromatic ring showed extensive hydrophobic interactions with residues
363 P287$^{7.36}$, I286$^{7.35}$, C187^{ECL2}, T290$^{7.39}$, A117$^{3.32}$ and M121$^{3.36}$ to stabilize the peptide
364 ligand in the binding pocket. S9 at the C-terminal end of the C9 peptide experienced
365 polar interactions extensively with S114$^{3.29}$, Q118$^{3.33}$ and R176$^{4.64}$ with oxygens in its
366 carbonyl and side chain. Of note, Q$^{3.33}$ is an amino acid residue conserved in some
367 chemoattractant GPCRs including FPR1 and FPR2 (Chen et al., 2022; Chen et al.,
368 2020; Zhu et al., 2022; Zhuang et al., 2020; Zhuang et al., 2022), suggesting the
369 presence of a common feature shared by this subclass of GPCRs. The aromatic ring
370 of F8 inserts deep into the binding pocket, pointing just above the “toggle switch”
371 W259$^{6.48}$ of GPR1 for G protein activation (Weis & Kobilka, 2018). By comparing the
372 structures of GPR1-C9 and CMKLR1-C9, the C9 peptide ligand was found to have
373 an average of 1.2 Å upward shift in GPR1, and the residues in contact with the
374 ligand were closer to the extracellular loop of GPR1 than CMKLR1 (Fig. S3). These
375 findings suggest that the binding site of C9 is shallower in GPR1 than in CMKLR1
376 despite the fact that the C9 peptide takes a similar pose in the binding pockets of
377 both receptors.
378
379 **Functional analysis of the GPR1-C9 interaction.**
380 Following the structural model of GPR1, site-directed mutagenesis of the receptor
381 was conducted to confirm the interactions between the C9 peptide and the receptor
382 binding pocket. Alanine substitutions of the key residues in the binding pocket of
383 GPR1 were performed, and the resulting receptors were expressed for functional
384 assays including cAMP inhibition and G protein dissociation to determine any
385 changes in GPR1 activation by the C9 peptide (Fig. 3). The results from these two
386 assays were consistent. Alanine substitution of residues forming polar interactions
387 with the C9 peptide, including N189^{ECL2}, E269$^{6.58}$, Y96$^{2.63}$, Y93$^{2.60}$, S114$^{3.29}$, Q118$^{3.33}$

388 and R176$^{4.64}$, resulted in a remarkable decrease in the potency of the ligand (Fig. 3,
389 A-C and E-G). Of note, the Y96$^{2.63}$A and E269$^{6.58}$A substitutions completely
390 diminished the responses. Both mutants expressed on the cell surface, thus
391 excluding global misfolding of the receptors after alanine substitution at these
392 positions. Functional assays revealed that, despite extensive polar interactions
393 between S9 in the C9 peptide and GPR1, single point mutations of S114$^{3.29}$,
394 Q118$^{3.33}$ or R176$^{4.64}$ did not completely eliminate the response. This result may be
395 explained by the flexibility at S9 where multiple hydrogen bonds may form alternately
396 between S114$^{3.29}$, Q118$^{3.33}$ or R176$^{4.64}$ of GPR1 and the carbonyl and side chain
397 oxygens of S9 (Fig. 3, A, B, E and F). Our prediction was confirmed after introducing
398 a triple-mutation at S114-Q118-R176, that completely abolished the agonist-induced
399 cAMP inhibition and G protein dissociation responses (Fig. 3, D and H). These
400 results altogether supported the role of the substituted amino acid residues in
401 hydrogen bond formation with P3, G4, Q5, F6 and S9 in the C9 peptide.
402
403 In addition to polar interactions, hydrophobic interactions also play an important role
404 in C9 interaction with GPR1. Mutations of selected nonpolar residues in the GPR1
405 binding pocket, including L186^{ECL2}, Y188^{ECL2}, Q283$^{7.32}$ and T290$^{7.39}$, reduced the
406 potency of C9-induced cAMP inhibition and G protein dissociation as shown in right-
407 shifted dose response curves (Fig. 3, C, D, G and H). Of note, the T290$^{7.39}$A
408 substitution nearly completely eliminated GPR1-mediated activation in the two
409 functional assays. Since this mutant was readily expressed on cell surface, it is
410 predicted that the side change of threonine may be important for interaction with F8
411 of the C9 peptide ligand. Overall, results from site-directed mutagenesis and
412 corresponding functional assays are in line with the cryo-EM structural model of the
413 C9-bound GPR1.
414
415 **Thermodynamic stability of GPR1-C9 interface**
416 Full-atom molecular dynamics (MD) simulations were performed for GPR1-C9
417 complex at room temperature (10 replicas of 1-μs-long simulation). In these MD
418 trajectories, the complex captured by cryo-EM were overall stable under
419 thermodynamic perturbation (Fig. S5), and the binding pose of the C9 peptide were
420 well kept through the assemble of 1-μs trajectories (Fig. 4 and Fig. S6). Except the
421 hydrophobic Phe (F2), all of the 9 residues in C9 peptide form hydrogen-bonds (H-

422 bonds) with GPR1 (Fig. 4). The residues close to the C-terminal end of the C9
423 peptide formed several H-bonds with Y96$^{2.63}$, N189^{ECL2}, R176$^{4.64}$, S114$^{3.29}$, Y262$^{6.51}$,
424 and K210$^{5.42}$. Among these, N189^{ECL2} and Y96$^{2.63}$ also formed H-bonds with P3 and
425 Q5 on the C9 peptide. The N-terminus of the peptide ligand was more likely to
426 interact with negatively charged E269$^{6.58}$. The latter also interacted with G4, while
427 the G4 formed a stable H-bond with R176$^{4.64}$ (Fig. 4B). These interactions resulted in
428 a complex network between C9 and the receptor, which rationalized the
429 thermodynamic stability of the C9 peptide in the binding pocket of GPR1.
430
431 Results of the MD simulations were correlated with functional assay data based on
432 the EC_{50} values of cAMP inhibition assays, using WT and alanine substituted
433 mutants of GPR1. Alanine substitution of N189^{ECL2} and Y96$^{2.63}$, which have the top 2
434 occupancy scores on single H-bond (Fig. 4A), abrogated cAMP inhibition (-logEC_{50} =
435 0), indicating their functional importance. Another functionally important residue is
436 E269$^{6.58}$, which has low single H-bond occupancy (<0.6, Fig. 4A) but the highest
437 overall H-bond occupancy (occupancy values >1.5) when all associated H-bonds
438 were considered. Its substitution with alanine led to loss of cAMP inhibition (Fig. 3C).
439 Therefore, there is a high-level correlation between the polar interactions of C9 with
440 GPR1 and its functions.
441
442 **Activation mechanism of the GPR1-Gi complex.**
443 To investigate the conformational changes associated with the activation of GPR1,
444 we compared the structure of active GPR1 and an antagonist-bound inactive C5aR
445 (C5aR-PMX53, PDB ID: 6C1R) for its homology to GPR1, or a C9-bound active
446 CMKLR1 (CMKLR1-C9, PDB ID: 7YKD), respectively (Fig. 5). The comparison
447 revealed an outward movement of TM5 and TM6, and an inward movement of TM7,
448 in the activation of GPR1 (Fig. 5A).Of note, the D$^{3.49}$-R$^{3.50}$-Y$^{3.51}$ motif found in most
449 Class A GPCRs for G protein activation, was replaced with D134-H135-Y136 in
450 GPR1. Previous reports indicate that polar interaction R$^{3.50}$ and Y$^{5.58}$ is important for
451 G protein activation (Wang et al., 2023; Weis & Kobilka, 2018; Zhou et al., 2019)
452 (Fig. 5B). However, the apparent activation of G proteins in C9-bound GPR1, which
453 only has H^{3,50} in this motif, suggests that the R$^{3.50}$-Y$^{5.58}$ interaction is not critical to G
454 protein activation. Supporting this notion, our substitution of H^{3,50} with Arg did not
455 significantly change G protein dissociation (Fig. 7D) but made the receptor less

capable of inhibiting cAMP (Fig. 7A). Alanine substitution of $H^{3,50}$ led to a complete loss of function (Fig. 7A and 7D). These results indicate that the $D^{3.49}$-$H^{3.50}$-$Y^{3.51}$ motif in the context of the overall sequence of GPR1 is functional in G protein activation, even in the absence of a $R^{3.50}$-$Y^{5.58}$ interaction.

The highly conserved residue $W259^{6.48}$ as a “toggle switch” of G protein activation showed an anti-clockwise rotation in GPR1-C9 structure (Fig. 5C), which is characteristic in other activated GPCRs (Weis & Kobilka, 2018; Zhou et al., 2019). For the $P^{5.50}$-I/$V^{3.40}$-$F^{6.44}$ motif, rotamer conformational changes was displayed in the GPR1-C9 structure in comparison with the inactive C5aR (Fig. 5D). To further identify the structural basis for different signaling responses of GPR1 and CMKLR1 upon C9 binding, we compared these active structures of the two receptors. An outward movement of TM5, TM7 and an inward movement of TM6 was demonstrated in both receptors upon C9 binding (Fig. 5E). As for the DRY motif, CMKLR1 presents a DRC in position and $R^{3.50}$ formed a polar interaction with the $Y^{5.58}$ residue (Fig. 5F). $H135^{3.50}$ in GPR1, however, pointed to the cytosolic direction with no observable polar interaction with adjacent receptor residues. For the “toggle switch”, $W259^{6.48}$ in GPR1 shifted slightly upwards (Fig. 5G). Not much difference in the orientation of the $P218^{5.50}$-$V125^{3.40}$-$F255^{6.44}$ motif was observed (Fig. 5H). Overall, despite differences in the geometry and important motifs between GPR1 and CMKLR1, GPR1 is able to activate the Gi proteins, albeit with a lower amplitude.

Next, the interaction between an activated GPR1 and the Gi class of heterotrimeric G proteins was examined. In this study, we adopted DNGαi1, a dominant negative form of human Gαi1 containing the G203A and A326S mutations for decreased affinity for nucleotide binding and increased stability of heterotrimeric G protein complex (Lee et al., 1992; Posner et al., 1998). In the structure, the α5 helix of Gαi inserted into the intracellular loops of GPR1, forming hydrophobic interactions with $F76^{2.43}$, $L151^{4.39}$, $V251^{6.40}$, $Y226^{5.58}$, $T247^{6.36}$, $K310^{8.49}$ (Fig. 6A). Of note, some polar interactions were found between α5 helix G352 and GPR1 $H135^{3.50}$, α5 helix N347 and GPR1 $H138^{3.53}$, αN helix R32 and GPR1 $H146^{ICL2}$ (Fig. 6A). Additionally, we also observed a hydrogen bond between GPR1 helix 8 and D312 of the Gβ subunit (Fig. 6B).

The interaction between the heterotrimeric Gi protein and the receptor was next compared with several Gi-coupled GPCRs including the active CMKLR1 and CCR5 (PDB ID: 7F1R), and the inactive C5aR and CXCR4 (PDB ID: 3ODU) (Fig. 6 C-E). The orientation of TM6 and TM7 marks the greatest difference between active and inactive receptors (Fig. 6 C and D). For the active receptors GPR1, CMKLR1 and CCR5, TM6 displayed an outward tilt allowing the space for interface between the receptor and the C-terminal α5 helix of Gαi (Fig. 6C). Helix8 of the active receptors showed a movement to the intracellular compartment for the engagement of the Gβ subunit (Fig. 6C). An inward movement of TM7 was also observed for GPR1 and other active receptors compared with the inactive representatives (Fig. 6D). Although we did not observe much polar interaction between GPR1 and the αN helix of Gαi as in CMKLR1 (Wang et al., 2023), the αN helix of Gαi moved upwards for a closer proximity with the receptor helix8 (Fig. 6E). These features contribute to the activation of G protein by GPR1.

We further verified the proposed mechanisms of G protein activation by introducing point mutations to the key residues. In addition to the substitution of H135$^{3.50}$ into the canonical arginine as mentioned above and shown in Fig. 7A, point mutations of P218$^{5.50}$-V125$^{3.40}$-F255$^{6.44}$ into alanine greatly reduced the cAMP inhibition as well as G protein dissociation (Fig. 7). Substitution of the “toggle switch” W259$^{6.48}$ with alanine caused a complete loss in cAMP inhibition, yet G protein dissociation was partially retained with a decreased efficacy and potency (Fig. 7 C and F). For the interaction interface between the receptor and Gαi, alanine substitution at H135$^{3.50}$, H138$^{3.53}$ and H146^{ICL2} completely diminished G protein dissociation and cAMP inhibition (Fig. 7 A-B and D-E). All these function assays confirmed the importance of aforementioned key residues in activating Gi proteins.

Discussion

There is increasing awareness of the importance of chemerin in immune regulation and lipid biogenesis, that are biological processes associated with a number of common illnesses including acute inflammation, psoriasis, angiogenesis, obesity, diabetes, nonalcoholic fatty liver disease, ovarian cancer and endometrial cancer (Bozaoglu et al., 2007; Ernst & Sinal, 2010; Goralski et al., 2019; Goralski et al., 2007; Helfer & Wu, 2018; Kennedy & Davenport, 2018; Macvanin et al., 2022; Parolini et al., 2007; Schioppa et al., 2020; Su et al., 2021; Sun et al., 2021; Yue et al., 2023). It is therefore critical to understand how chemerin exerts these physiological and pathological functions through the chemerin receptors. To date, three chemerin receptors have been identified. CMKLR1 is well known for its role in mediating most biological activities of chemerin, and CCRL2 is a non-functional chemerin receptor serving as a scavenger of excess chemerin (Kennedy & Davenport, 2018). In comparison, the functions of GPR1 are less clear. Initially identified as an orphan receptor (Marchese et al., 1994), the natural ligand of GPR1 was not clear until 2008, when Barnea *et al* reported chemerin-induced membrane association of β-arrestin2 using Tango, a functional assay for protein-protein interaction (Barnea et al., 2008). In this functional assay, chemerin was more potent on GPR1 (EC_{50} of 240 pM) than on CMKLR1 (3 nM). The same also applied to the C9 peptide, that showed a higher potency (EC_{50} of 1 nM) on GPR1 than on CMKLR1 (24 nM). Although GPR1 was considered a receptor for activating the β-arrestin2 pathway (Barnea et al., 2008; Fischer et al., 2021), in some studies GPR1-mediated G protein activation was reported (De Henau et al., 2016; Degroot et al., 2022).

In this study, we present a cryo-EM structure of the C9-peptide bond GPR1-Gi protein complex. This study takes advantage of the finding that, unlike CMKLR1 that uses the N-terminal extracellular domain for stable binding of full-length chemerin in addition to receptor interaction with the C-terminal nonapeptide (C9), GPR1 uses only the binding pocket formed by the 7 transmembrane domains for interaction with the C-terminal peptide (Fischer et al., 2021). It is therefore well justified to use C9 for GPR1 complex formation. Our structural model provides molecular insights into the mode of binding between C9 and GPR1. In this model, C9 takes an “S”-shape pose in the binding pocket. The binding pocket is formed mainly by TM2, 3, 4, 6, 7 and

553 deep enough to accommodate the nonapeptide, with its C terminal S9 reaching the
554 bottom of the binding pocket and forming extensive polar interactions with S114$^{3.29}$,
555 Q118$^{3.33}$ and R176$^{4.64}$. This model differs from the proposed model by Fischer et al
556 that was developed through homology modelling and molecular docking (Fischer et
557 al., 2021). In the Fischer model, the C9 binding to GPR1 is dominated by
558 hydrophobic interactions between F8 of the ligand and a hydrophobic domain in the
559 extracellular loop 2 of GPR1 consisting of F$^{4.69}$, L$^{4.74}$, Y$^{4.76}$, and F$^{4.79}$. This feature,
560 combined with a proposed hydrophobic interaction between F6 and F$^{2.68}$, renders a
561 shallow hydrophobic pocket for ligand binding involving mostly the extracellular
562 domains as seen in many chemokine receptors. As a result, the C-terminal S9 of the
563 ligand was found barely interacting with the receptor. For ligand accommodation in
564 the Fischer model, the peptide ligand bended between G4 and Q5, pointing towards
565 T$^{7.39}$. Apparently this is not consistent with the cryo-EM model in this study, as both
566 the molecular dynamics data and alanine substitution of key residues support an
567 interaction between the C-terminal amino acids of the ligand and amino acid
568 residues at the bottom of the binding pocket.
569
570 Our structural model provides direct evidence for an interaction of GPR1 and the Gi
571 proteins, that forms the foundation of G protein signaling through GPR1. Analysis of
572 the receptor-Gi protein interface found some polar interactions between the receptor
573 and G protein heterodimer complex. Of note, the highly G protein-binding motif,
574 D$^{3.49}$-R$^{3.50}$-Y$^{3.51}$, found in many class A GPCRs, is replaced by DHY in GPR1.
575 However, histamine substitution in this motif did not diminish G protein binding, and
576 a polar interaction between H135$^{3.50}$ and α5 helix of Gi was evident. This structural
577 feature indicates that the DRY motif is not absolutely necessary for GPCR-Gi
578 interaction, and the actual coupling of the receptor to G protein may be context-
579 specific in each of the receptors.
580
581 The C9-GPR1-Gi complex structure was compared with the C9-CMKLR1-structure
582 that we resolved earlier (Wang et al., 2023). They show high degrees of homology at
583 both primary sequence level (71% sequence homology, with 37% identical amino
584 acids) (Kennedy & Davenport, 2018) and 3D structure level. For G protein interacting
585 interface, CMKLR1 has additional polar interactions with the αN helix of Gαi than
586 GPR1. The difference in DRY motif (DRC in CMKLR1, DHY in GPR1) does not

587 seem to affect Gi coupling in pharmacological term. Another structural feature, the
588 absence of the polar interaction in GPR1 between $H^{3.50}$ and $Y^{5.58}$ (due to the $R^{3.50}$ to
589 $H^{3.50}$ switch), does not produce a functional impact in Gi coupling. Of importance, the
590 overall receptor structure does not change due to the $R^{3.50}$ to $H^{3.50}$ switch. Hence,
591 the lower G protein coupling efficiency in GPR1 may be explained by fewer
592 interactions at the receptor-Gαi interface, but not the $R^{3.50}$ to $H^{3.50}$ switch as
593 predicted before the structure was resolved. For the receptor-C9 interaction, the C9
594 peptide resumes an "S" shape in both GPR1 and CMKLR1. However, C9 insertion
595 into the GPR1 binding pocket is not as deep as it is in CMKLR1, showing an average
596 of 1.2Å upward shift in GPR1. As a result, the bottom of the GPR1 binding pocket is
597 further above $W^{6.48}$, the 'toggle switch' for G protein activation, when compared with
598 CMKLR1 (Wang et al., 2023) . It is however much deeper than the predicted model
599 by Fischer et al (Fischer et al., 2021). Taken together, structural analysis of the C9-
600 GPR1-Gi complex provides evidence that GPR1 is fully capable of activating Gi
601 proteins despite minor sequence differences at the DRY motif and a shallower
602 binding pocket for the peptide ligand.
603
604 While the structural information of GPR1 expands our knowledge in chemerin
605 receptor biology, several unknowns still remain for further investigation. Given the
606 high similarities between GPR1 and CMKLR1, they may share a variety of agonists
607 and antagonists. Currently the only natural ligand of GPR1 and CMKLR1 is
608 chemerin, and the wide distribution of GPR1 and CMKLR1 among immune cells,
609 adipose tissues and central nervous system suggests the presence of other possible
610 endogenous ligands (Herova et al., 2015; Marchese et al., 1994; Tokizawa et al.,
611 2000; Wittamer et al., 2003; Wittamer et al., 2004). Indeed, a previous report
612 unraveled a novel ligand of GPR1, FAM19A1, which is highly expressed in adult
613 hippocampus and has neural modulatory effect (Zheng et al., 2018). However, the
614 reported study was based primarily on animal experiments without a biochemical
615 mechanism for receptor activation, and there is still a lack of structural information
616 about FAM19A1 interaction with GPR1. Another unresolved issue is whether GPR1
617 and CMKLR1 differ in activating the β-arrestin pathway, as currently there is a lack of
618 structure for a ligand-bound receptor-β-arrestin complex. Further investigation in
619 these directions will help to understand how the signals generated by chemerin
620 binding are mediated by these two receptors.

Acknowledgments

This work was supported in part by grants from the Science, Technology and Innovation Commission of Shenzhen Municipality GXWD20201231105722002-20200831175432002 (R.D.Y., Y.D. and L.Z.), JCYJ20200109150019113 (Y.D., G.C.), JCYJ20200109150003938 (L.Z.), RCYX20200714114645019 (L.Z.) and RCBS20221008093330067 (A.L.). This work was also supported by National Natural Science Foundation of China 31971179 (L.Z.), 32271263 (Y.D.) and 32070950 (R.D.Y.), the Fellowship of China Postdoctoral Science Foundation 2022M713049 (A.L.) and 2021M703092 (J. W.), the Ganghong Young Scholar Development Fund (R.D.Y.), the Kobilka Institute of Innovative Drug Discovery at The Chinese University of Hong Kong, Shenzhen (Y.D., R.D.Y.), and the fund from Shenzhen-Hong Kong Cooperation Zone for Technology and Innovation (HZQB-KCZYB-2020056). The authors thank the Kobilka Cryo-Electron Microscopy Center in the Chinese University of Hong Kong, Shenzhen for cryo-electron microscopy analysis. The computational work was supported by the Warshel Institute for Computational Biology (funding from Shenzhen City and Longgang District).

Author Contributions

A.L. performed cloning, protein expression and purification of the human GPR1 protein for complex formation, screening of cryo-EM grids, collection of cryo-EM data and building of the structural model; Y.L. conducted mutagenesis analysis, functional assays, structural comparison and figure preparation; G.C. assisted in structural model building; W.L. and L.Z. performed MD simulation; J.W. designed Nano-BiT assay and provided constructs used in this study; Q.L. performed initial modelling and functional assays; F.Y. provided purified G proteins; Y.D. and R.D.Y. designed and supervised the research; Y.L. and R.D.Y. wrote the manuscript.

Competing Interest Statement

The authors declare no competing interest.

References:

Anandakrishnan, R., Aguilar, B., & Onufriev, A. V. (2012). H++ 3.0: automating pK prediction and the preparation of biomolecular structures for atomistic molecular modeling and simulations. *Nucleic Acids Res*, *40*(Web Server issue), W537-541. https://doi.org/10.1093/nar/gks375

Ballesteros, J. A., & Weinstein, H. (1995). Integrated methods for the construction of three-dimensional models and computational probing of structure-function relations in G protein-coupled receptors. In *Methods in neurosciences* (Vol. 25, pp. 366-428). Elsevier.

Barnea, G., Strapps, W., Herrada, G., Berman, Y., Ong, J., Kloss, B., Axel, R., & Lee, K. J. (2008). The genetic design of signaling cascades to record receptor activation. *Proc Natl Acad Sci U S A*, *105*(1), 64-69. https://doi.org/10.1073/pnas.0710487105

Bozaoglu, K., Bolton, K., McMillan, J., Zimmet, P., Jowett, J., Collier, G., Walder, K., & Segal, D. (2007). Chemerin is a novel adipokine associated with obesity and metabolic syndrome. *Endocrinology*, *148*(10), 4687-4694. https://doi.org/10.1210/en.2007-0175

Caulfield, M., Munroe, P., Pembroke, J., Samani, N., Dominiczak, A., Brown, M., Benjamin, N., Webster, J., Ratcliffe, P., O'Shea, S., Papp, J., Taylor, E., Dobson, R., Knight, J., Newhouse, S., Hooper, J., Lee, W., Brain, N., Clayton, D., . . . Study, M. R. C. B. G. o. H. (2003). Genome-wide mapping of human loci for essential hypertension. *Lancet*, *361*(9375), 2118-2123. https://doi.org/10.1016/S0140-6736(03)13722-1

Chen, G., Wang, X., Liao, Q., Ge, Y., Jiao, H., Chen, Q., Liu, Y., Lyu, W., Zhu, L., van Zundert, G. C. P., Robertson, M. J., Skiniotis, G., Du, Y., Hu, H., & Ye, R. D. (2022). Structural basis for recognition of N-formyl peptides as pathogen-associated molecular patterns. *Nat Commun*, *13*(1), 5232. https://doi.org/10.1038/s41467-022-32822-y

Chen, T., Xiong, M., Zong, X., Ge, Y., Zhang, H., Wang, M., Won Han, G., Yi, C., Ma, L., Ye, R. D., Xu, Y., Zhao, Q., & Wu, B. (2020). Structural basis of ligand binding modes at the human formyl peptide receptor 2. *Nat Commun*, *11*(1), 1208. https://doi.org/10.1038/s41467-020-15009-1

Chun, E., Thompson, A. A., Liu, W., Roth, C. B., Griffith, M. T., Katritch, V., Kunken, J., Xu, F., Cherezov, V., Hanson, M. A., & Stevens, R. C. (2012). Fusion partner toolchest for the stabilization and crystallization of G protein-coupled receptors. *Structure*, *20*(6), 967-976. https://doi.org/10.1016/j.str.2012.04.010

De Henau, O., Degroot, G. N., Imbault, V., Robert, V., De Poorter, C., McHeik, S., Gales, C., Parmentier, M., & Springael, J. Y. (2016). Signaling Properties of Chemerin Receptors CMKLR1, GPR1 and CCRL2. *PLoS One*, *11*(10), e0164179. https://doi.org/10.1371/journal.pone.0164179

Degroot, G. N., Lepage, V., Parmentier, M., & Springael, J. Y. (2022). The Atypical Chemerin Receptor GPR1 Displays Different Modes of Interaction with beta-Arrestins in Humans and Mice with Important Consequences on Subcellular Localization and Trafficking. *Cells*, *11*(6). https://doi.org/10.3390/cells11061037

Ernst, M. C., & Sinal, C. J. (2010). Chemerin: at the crossroads of inflammation and obesity. *Trends Endocrinol Metab*, *21*(11), 660-667. https://doi.org/10.1016/j.tem.2010.08.001

697 Fischer, T. F., Czerniak, A. S., Weiß, T., Schoeder, C. T., Wolf, P., Seitz, O., Meiler,
698 J., & Beck-Sickinger, A. G. (2021). Ligand-binding and -scavenging of the
699 chemerin receptor GPR1. *Cellular and Molecular Life Sciences*, *78*(17-18),
700 6265-6281. https://doi.org/10.1007/s00018-021-03894-8
701 Goralski, K. B., Jackson, A. E., McKeown, B. T., & Sinal, C. J. (2019). More Than an
702 Adipokine: The Complex Roles of Chemerin Signaling in Cancer. *Int J Mol*
703 *Sci*, *20*(19). https://doi.org/10.3390/ijms20194778
704 Goralski, K. B., McCarthy, T. C., Hanniman, E. A., Zabel, B. A., Butcher, E. C.,
705 Parlee, S. D., Muruganandan, S., & Sinal, C. J. (2007). Chemerin, a novel
706 adipokine that regulates adipogenesis and adipocyte metabolism. *J Biol*
707 *Chem*, *282*(38), 28175-28188. https://doi.org/10.1074/jbc.M700793200
708 Helfer, G., & Wu, Q. F. (2018). Chemerin: a multifaceted adipokine involved in
709 metabolic disorders. *J Endocrinol*, *238*(2), R79-R94.
710 https://doi.org/10.1530/JOE-18-0174
711 Herova, M., Schmid, M., Gemperle, C., & Hersberger, M. (2015). ChemR23, the
712 receptor for chemerin and resolvin E1, is expressed and functional on M1 but
713 not on M2 macrophages. *J Immunol*, *194*(5), 2330-2337.
714 https://doi.org/10.4049/jimmunol.1402166
715 Huang, J., Rauscher, S., Nawrocki, G., Ran, T., Feig, M., de Groot, B. L.,
716 Grubmuller, H., & MacKerell, A. D., Jr. (2017). CHARMM36m: an improved
717 force field for folded and intrinsically disordered proteins. *Nat Methods*, *14*(1),
718 71-73. https://doi.org/10.1038/nmeth.4067
719 Inoue, A., Raimondi, F., Kadji, F. M. N., Singh, G., Kishi, T., Uwamizu, A., Ono, Y.,
720 Shinjo, Y., Ishida, S., Arang, N., Kawakami, K., Gutkind, J. S., Aoki, J., &
721 Russell, R. B. (2019). Illuminating G-Protein-Coupling Selectivity of GPCRs.
722 *Cell*, *177*(7), 1933-1947 e1925. https://doi.org/10.1016/j.cell.2019.04.044
723 Karagiannis, G. S., Weile, J., Bader, G. D., & Minta, J. (2013). Integrative pathway
724 dissection of molecular mechanisms of moxLDL-induced vascular smooth
725 muscle phenotype transformation. *BMC Cardiovasc Disord*, *13*, 4.
726 https://doi.org/10.1186/1471-2261-13-4
727 Kennedy, A. J., & Davenport, A. P. (2018). International Union of Basic and Clinical
728 Pharmacology CIII: Chemerin Receptors CMKLR1 (Chemerin1) and GPR1
729 (Chemerin2) Nomenclature, Pharmacology, and Function. *Pharmacol Rev*,
730 *70*(1), 174-196. https://doi.org/10.1124/pr.116.013177
731 Lee, E., Taussig, R., & Gilman, A. G. (1992). The G226A mutant of Gs alpha
732 highlights the requirement for dissociation of G protein subunits. *J Biol Chem*,
733 *267*(2), 1212-1218. https://www.ncbi.nlm.nih.gov/pubmed/1730644
734 Lehrke, M., Becker, A., Greif, M., Stark, R., Laubender, R. P., von Ziegler, F.,
735 Lebherz, C., Tittus, J., Reiser, M., Becker, C., Goke, B., Leber, A. W.,
736 Parhofer, K. G., & Broedl, U. C. (2009). Chemerin is associated with markers
737 of inflammation and components of the metabolic syndrome but does not
738 predict coronary atherosclerosis. *Eur J Endocrinol*, *161*(2), 339-344.
739 https://doi.org/10.1530/EJE-09-0380
740 Macvanin, M. T., Rizzo, M., Radovanovic, J., Sonmez, A., Paneni, F., & Isenovic, E.
741 R. (2022). Role of Chemerin in Cardiovascular Diseases. *Biomedicines*,
742 *10*(11). https://doi.org/10.3390/biomedicines10112970
743 Maeda, S., Koehl, A., Matile, H., Hu, H., Hilger, D., Schertler, G. F. X., Manglik, A.,
744 Skiniotis, G., Dawson, R. J. P., & Kobilka, B. K. (2018). Development of an
745 antibody fragment that stabilizes GPCR/G-protein complexes. *Nat Commun*,
746 *9*(1), 3712. https://doi.org/10.1038/s41467-018-06002-w

Marchese, A., Docherty, J. M., Nguyen, T., Heiber, M., Cheng, R., Heng, H. H., Tsui, L. C., Shi, X., George, S. R., & O'Dowd, B. F. (1994). Cloning of human genes encoding novel G protein-coupled receptors. *Genomics*, *23*(3), 609-618. https://doi.org/10.1006/geno.1994.1549

Meder, W., Wendland, M., Busmann, A., Kutzleb, C., Spodsberg, N., John, H., Richter, R., Schleuder, D., Meyer, M., & Forssmann, W. G. (2003). Characterization of human circulating TIG2 as a ligand for the orphan receptor ChemR23. *FEBS Lett*, *555*(3), 495-499. https://doi.org/10.1016/s0014-5793(03)01312-7

Neves, K. B., Nguyen Dinh Cat, A., Alves-Lopes, R., Harvey, K. Y., Costa, R. M. D., Lobato, N. S., Montezano, A. C., Oliveira, A. M., Touyz, R. M., & Tostes, R. C. (2018). Chemerin receptor blockade improves vascular function in diabetic obese mice via redox-sensitive and Akt-dependent pathways. *Am J Physiol Heart Circ Physiol*, *315*(6), H1851-H1860. https://doi.org/10.1152/ajpheart.00285.2018

Parolini, S., Santoro, A., Marcenaro, E., Luini, W., Massardi, L., Facchetti, F., Communi, D., Parmentier, M., Majorana, A., Sironi, M., Tabellini, G., Moretta, A., & Sozzani, S. (2007). The role of chemerin in the colocalization of NK and dendritic cell subsets into inflamed tissues. *Blood*, *109*(9), 3625-3632. https://doi.org/10.1182/blood-2006-08-038844

Posner, B. A., Mixon, M. B., Wall, M. A., Sprang, S. R., & Gilman, A. G. (1998). The A326S mutant of Gialpha1 as an approximation of the receptor-bound state. *J Biol Chem*, *273*(34), 21752-21758. https://doi.org/10.1074/jbc.273.34.21752

Rourke, J. L., Dranse, H. J., & Sinal, C. J. (2015). CMKLR1 and GPR1 mediate chemerin signaling through the RhoA/ROCK pathway. *Mol Cell Endocrinol*, *417*, 36-51. https://doi.org/10.1016/j.mce.2015.09.002

Rourke, J. L., Muruganandan, S., Dranse, H. J., McMullen, N. M., & Sinal, C. J. (2014). Gpr1 is an active chemerin receptor influencing glucose homeostasis in obese mice. *J Endocrinol*, *222*(2), 201-215. https://doi.org/10.1530/JOE-14-0069

Samson, M., Edinger, A. L., Stordeur, P., Rucker, J., Verhasselt, V., Sharron, M., Govaerts, C., Mollereau, C., Vassart, G., Doms, R. W., & Parmentier, M. (1998). ChemR23, a putative chemoattractant receptor, is expressed in monocyte-derived dendritic cells and macrophages and is a coreceptor for SIV and some primary HIV-1 strains. *Eur J Immunol*, *28*(5), 1689-1700. https://doi.org/10.1002/(SICI)1521-4141(199805)28:05<1689::AID-IMMU1689>3.0.CO;2-I

Schioppa, T., Sozio, F., Barbazza, I., Scutera, S., Bosisio, D., Sozzani, S., & Del Prete, A. (2020). Molecular Basis for CCRL2 Regulation of Leukocyte Migration. *Front Cell Dev Biol*, *8*, 615031. https://doi.org/10.3389/fcell.2020.615031

Shimizu, N., Tanaka, A., Oue, A., Mori, T., Ohtsuki, T., Apichartpiyakul, C., Uchiumi, H., Nojima, Y., & Hoshino, H. (2009). Broad usage spectrum of G protein-coupled receptors as coreceptors by primary isolates of HIV. *AIDS*, *23*(7), 761-769. https://doi.org/10.1097/QAD.0b013e328326cc0d

Su, X., Cheng, Y., Zhang, G., & Wang, B. (2021). Chemerin in inflammatory diseases. *Clin Chim Acta*, *517*, 41-47. https://doi.org/10.1016/j.cca.2021.02.010

Sun, J. X., Zhang, C., Cheng, Z. B., Tang, M. Y., Liu, Y. Z., Jiang, J. F., Xiao, X., & Huang, L. (2021). Chemerin in atherosclerosis. *Clin Chim Acta*, *520*, 8-15. https://doi.org/10.1016/j.cca.2021.05.015

Tokizawa, S., Shimizu, N., Hui-Yu, L., Deyu, F., Haraguchi, Y., Oite, T., & Hoshino, H. (2000). Infection of mesangial cells with HIV and SIV: identification of GPR1 as a coreceptor. *Kidney Int*, *58*(2), 607-617. https://doi.org/10.1046/j.1523-1755.2000.00207.x

Wang, J., Chen, G., Liao, Q., Lyu, W., Liu, A., Zhu, L., Du, Y., & Ye, R. D. (2023). Cryo-EM structure of the human chemerin receptor 1-Gi protein complex bound to the C-terminal nonapeptide of chemerin. *Proc Natl Acad Sci U S A*, *120*(11), e2214324120. https://doi.org/10.1073/pnas.2214324120

Weis, W. I., & Kobilka, B. K. (2018). The Molecular Basis of G Protein-Coupled Receptor Activation. *Annu Rev Biochem*, *87*, 897-919. https://doi.org/10.1146/annurev-biochem-060614-033910

Wittamer, V., Franssen, J. D., Vulcano, M., Mirjolet, J. F., Le Poul, E., Migeotte, I., Brezillon, S., Tyldesley, R., Blanpain, C., Detheux, M., Mantovani, A., Sozzani, S., Vassart, G., Parmentier, M., & Communi, D. (2003). Specific recruitment of antigen-presenting cells by chemerin, a novel processed ligand from human inflammatory fluids. *J Exp Med*, *198*(7), 977-985. https://doi.org/10.1084/jem.20030382

Wittamer, V., Gregoire, F., Robberecht, P., Vassart, G., Communi, D., & Parmentier, M. (2004). The C-terminal nonapeptide of mature chemerin activates the chemerin receptor with low nanomolar potency. *J Biol Chem*, *279*(11), 9956-9962. https://doi.org/10.1074/jbc.M313016200

Yue, G., An, Q., Xu, X., Jin, Z., Ding, J., Hu, Y., Du, Q., Xu, J., & Xie, R. (2023). The role of Chemerin in human diseases. *Cytokine*, *162*, 156089. https://doi.org/10.1016/j.cyto.2022.156089

Zabel, B. A., Allen, S. J., Kulig, P., Allen, J. A., Cichy, J., Handel, T. M., & Butcher, E. C. (2005). Chemerin activation by serine proteases of the coagulation, fibrinolytic, and inflammatory cascades. *J Biol Chem*, *280*(41), 34661-34666. https://doi.org/10.1074/jbc.M504868200

Zabel, B. A., Nakae, S., Zuniga, L., Kim, J. Y., Ohyama, T., Alt, C., Pan, J., Suto, H., Soler, D., Allen, S. J., Handel, T. M., Song, C. H., Galli, S. J., & Butcher, E. C. (2008). Mast cell-expressed orphan receptor CCRL2 binds chemerin and is required for optimal induction of IgE-mediated passive cutaneous anaphylaxis. *J Exp Med*, *205*(10), 2207-2220. https://doi.org/10.1084/jem.20080300

Zabel, B. A., Silverio, A. M., & Butcher, E. C. (2005). Chemokine-like receptor 1 expression and chemerin-directed chemotaxis distinguish plasmacytoid from myeloid dendritic cells in human blood. *J Immunol*, *174*(1), 244-251. https://doi.org/10.4049/jimmunol.174.1.244

Zheng, C., Chen, D., Zhang, Y., Bai, Y., Huang, S., Zheng, D., Liang, W., She, S., Peng, X., Wang, P., Mo, X., Song, Q., Lv, P., Huang, J., Ye, R. D., & Wang, Y. (2018). FAM19A1 is a new ligand for GPR1 that modulates neural stem-cell proliferation and differentiation. *FASEB J*, fj201800020RRR. https://doi.org/10.1096/fj.201800020RRR

Zhou, Q., Yang, D., Wu, M., Guo, Y., Guo, W., Zhong, L., Cai, X., Dai, A., Jang, W., Shakhnovich, E. I., Liu, Z. J., Stevens, R. C., Lambert, N. A., Babu, M. M., Wang, M. W., & Zhao, S. (2019). Common activation mechanism of class A GPCRs. *Elife*, *8*. https://doi.org/10.7554/eLife.50279

Zhu, Y., Lin, X., Zong, X., Han, S., Wang, M., Su, Y., Ma, L., Chu, X., Yi, C., Zhao, Q., & Wu, B. (2022). Structural basis of FPR2 in recognition of Abeta42 and neuroprotection by humanin. *Nat Commun*, *13*(1), 1775. https://doi.org/10.1038/s41467-022-29361-x

Zhuang, Y., Liu, H., Edward Zhou, X., Kumar Verma, R., de Waal, P. W., Jang, W., Xu, T. H., Wang, L., Meng, X., Zhao, G., Kang, Y., Melcher, K., Fan, H., Lambert, N. A., Eric Xu, H., & Zhang, C. (2020). Structure of formylpeptide receptor 2-Gi complex reveals insights into ligand recognition and signaling. *Nat Commun*, *11*(1), 885. https://doi.org/10.1038/s41467-020-14728-9

Zhuang, Y., Wang, L., Guo, J., Sun, D., Wang, Y., Liu, W., Xu, H. E., & Zhang, C. (2022). Molecular recognition of formylpeptides and diverse agonists by the formylpeptide receptors FPR1 and FPR2. *Nat Commun*, *13*(1), 1054. https://doi.org/10.1038/s41467-022-28586-0

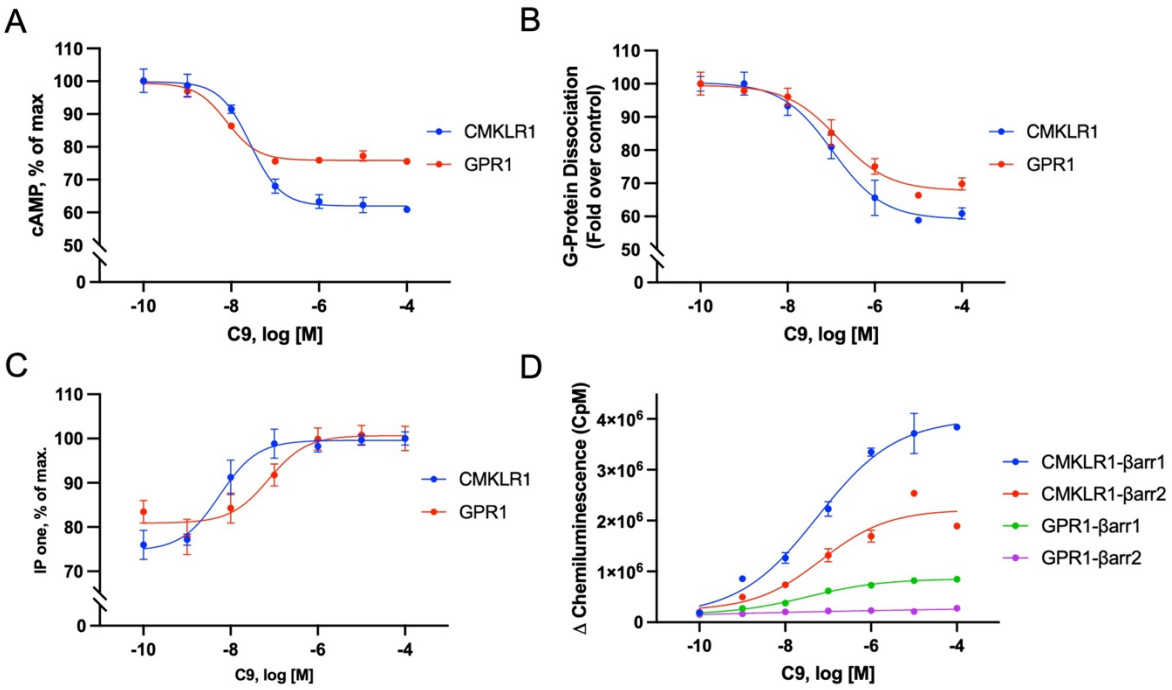

Figure 1. cAMP inhibition, G protein dissociation, IP1 accumulation and β-arrestin recruitment in response to different concentrations of C9. Cells expressing GPR1 (red) and CMKLR1 (blue) were examined in different assays including **(A)** cAMP inhibition, **(B)** NanoBiT-based G protein dissociation, **(C)** Accumulation of IP1, and NanoBiT-based β-arrestin recruitment. Both β-arrestin1 (blue, green) and β-arrestin2 (red, purple) were examined. Data are shown as means ± SEM from three independent experiments.

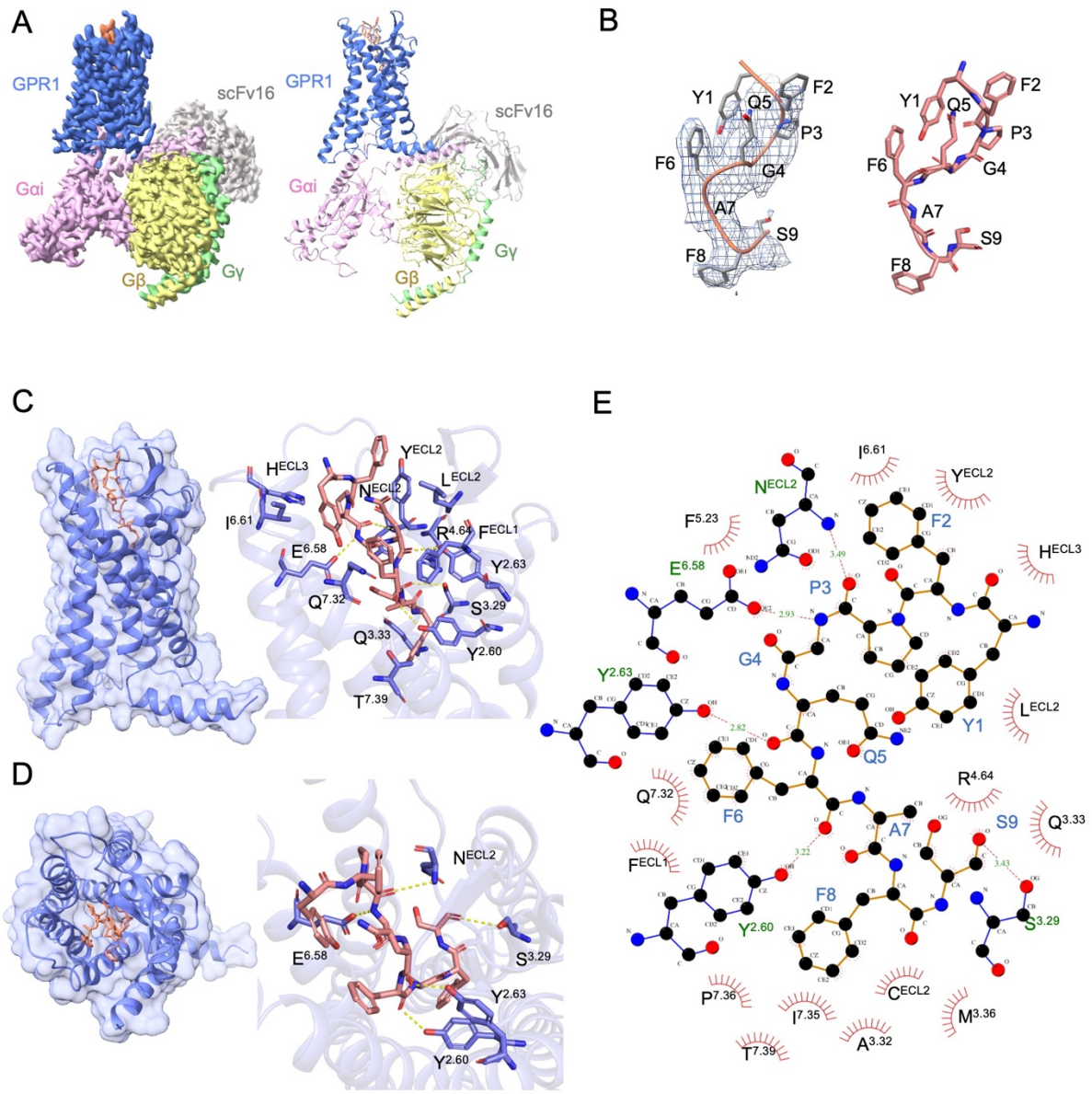

Figure 2. Overall structure and ligand binding pocket of C9-GPR1-Gi complex. (A) Cryo-EM density map (left) and the structural model (right) of the GPR1-Gi-scFv16 complex bound to C9. **(B)** Cryo-EM density map (left) and the pose of C9 peptide backbone (right) in the GPR1 binding pocket. Amino acid residues of C9 are marked in single letters and position numbers. **(C-E)** Interactions of C9 with amino acid residues in the GPR1 binding pocket, shown in side view (C), extracellular view (D) and LigPlot+ 2D representation (E). In the overall structures, the receptor (marine blue) is shown in cartoon and surface representation. The C9 peptide is shown in sticks with carbon in salmon orange. The residues of GPR1 within 4 Å from the C9 peptide (salmon orange licorice and ribbon) are shown in marine blue licorice. The hydrogen bonds are displayed as dashed lines. The residue numbering of GPR1 follows the Ballesteros–Weinstein nomenclature.

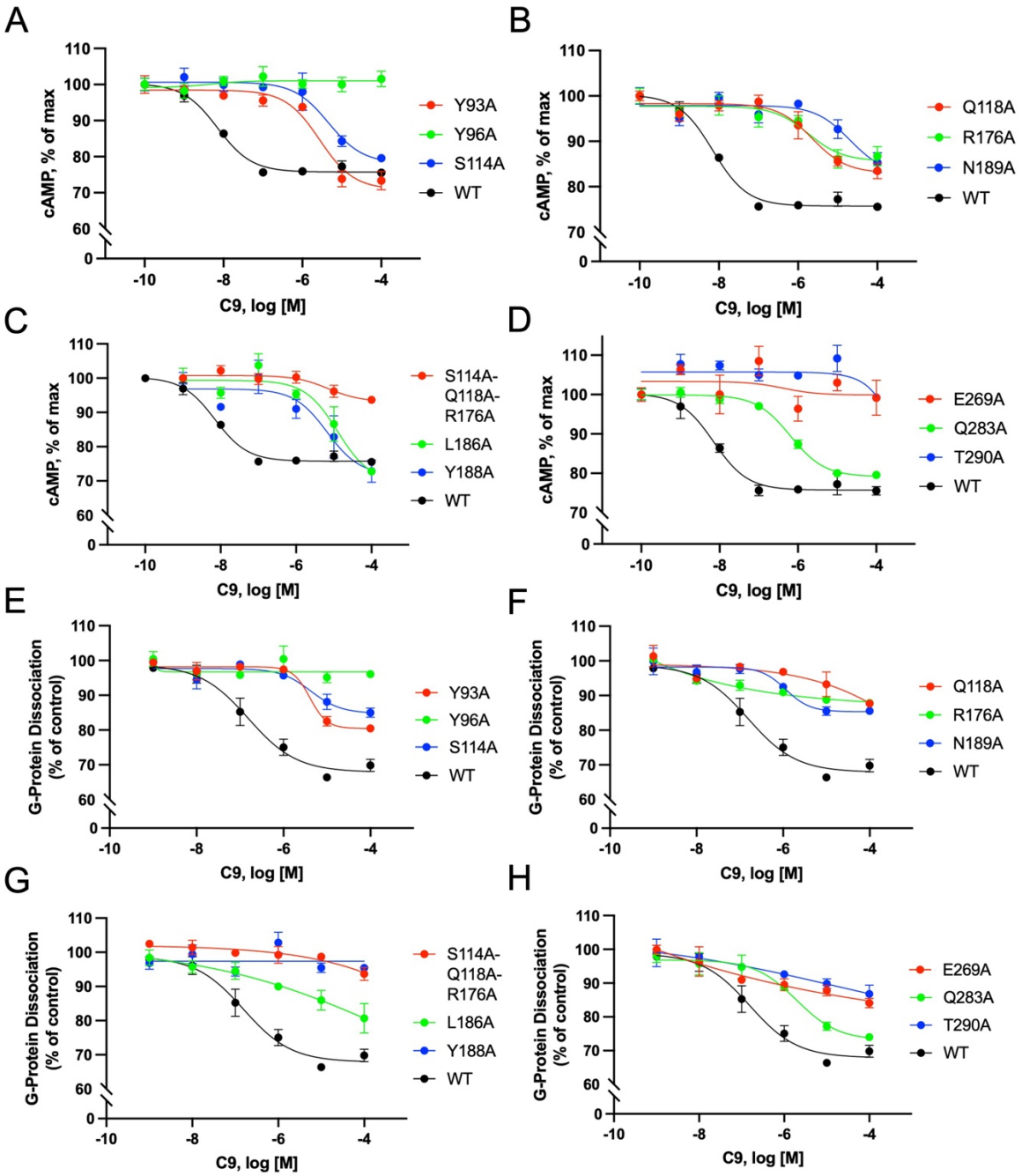

Figure 3. Structural mutants of C9-GPR1 binding pocket affect ligand-induced cAMP inhibition and G protein dissociation. (A - D) cAMP response in HeLa cells transfected to express WT or mutant GPR1. Different concentrations of C9 are applied. **(E - H)** G protein dissociation in HEK293T cells co-transfected to express WT or mutant GPR1, Gαi1-LgBiT, Gβ1, and SmBiT-Gγ2. Different concentrations of C9 are applied. All data shown are means ± SEM from three independent experiments.

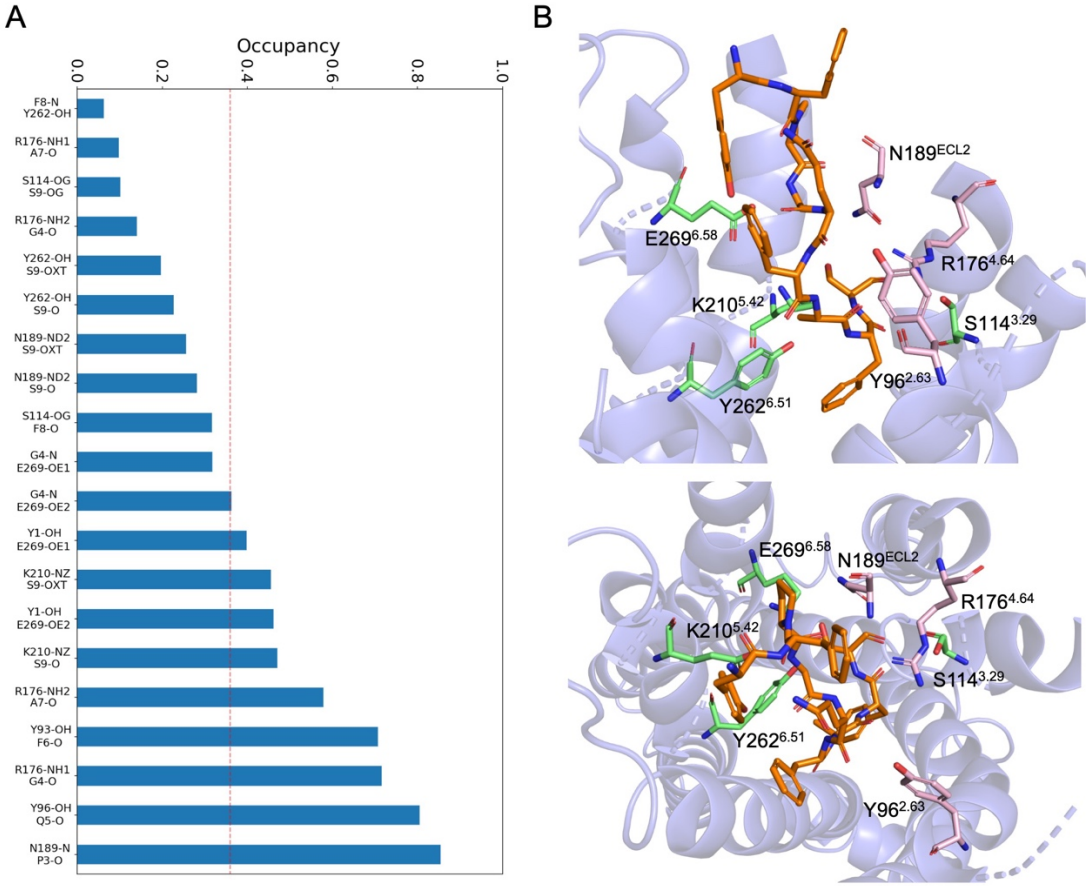

Figure 4. Thermodynamic stability analysis of the GPR1-C9 interface with µs-scale MD simulations. (A) The occupancy of all H-bonds between C9 and GPR1 observed in MD simulations. **(B)** Side view (upper panel) and top view (lower panel) of the distributions of functionally related residues around the C9 peptide.

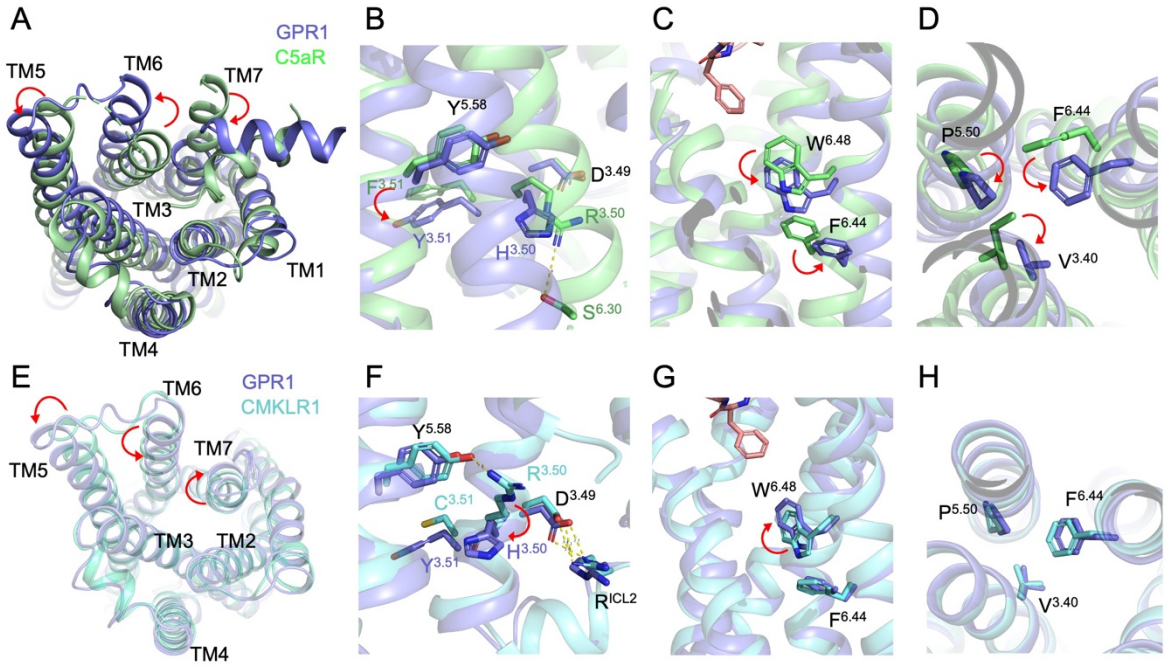

Figure 5. Comparison of GPCR structural motifs for G protein activation. (A) Intracellular view of the movement of GPR1 transmembrane helix 5, 6, and 7 (shown in marine blue) in comparison with inactive C5aR (PDB ID: 6C1R, shown in lime green). **(B)** Side close-up view of the $D^{3.49}$-$R^{3.50}$-$Y^{3.51}$ motif. A downward movement of $Y^{3.51}$ of GPR1 is highlighted by a red arrow. **(C)** Side close-up view of the "toggle switch", $W^{6.48}$ and $F^{6.44}$, an anti-clockwise rotation is highlighted for GPR1. **(D)** Rotamer conformational changes at the $P^{5.50}$-$I/V^{3.40}$-$F^{6.44}$ motif of GPR1 and C5aR, respectively. **(E)** Intracellular view of the movement of GPR1 transmembrane helix 5, 6, and 7 (shown in marine blue) in comparison with active CMKLR1 (PDB ID: 7YKD, shown in cyan). **(F)** Side close-up view of the $D^{3.49}$-$R^{3.50}$-$Y^{3.51}$ motif. A downward movement of $H^{3.50}$ of GPR1 is highlighted by a red arrow. **(G)** Side close-up view of the "toggle switch", $W^{6.48}$ and $F^{6.44}$, a clockwise rotation is highlighted for GPR1. **(H)** No significant conformational change at $P^{5.50}$-$I/V^{3.40}$-$F^{6.44}$ motif of GPR1 and CMKLR1, respectively.

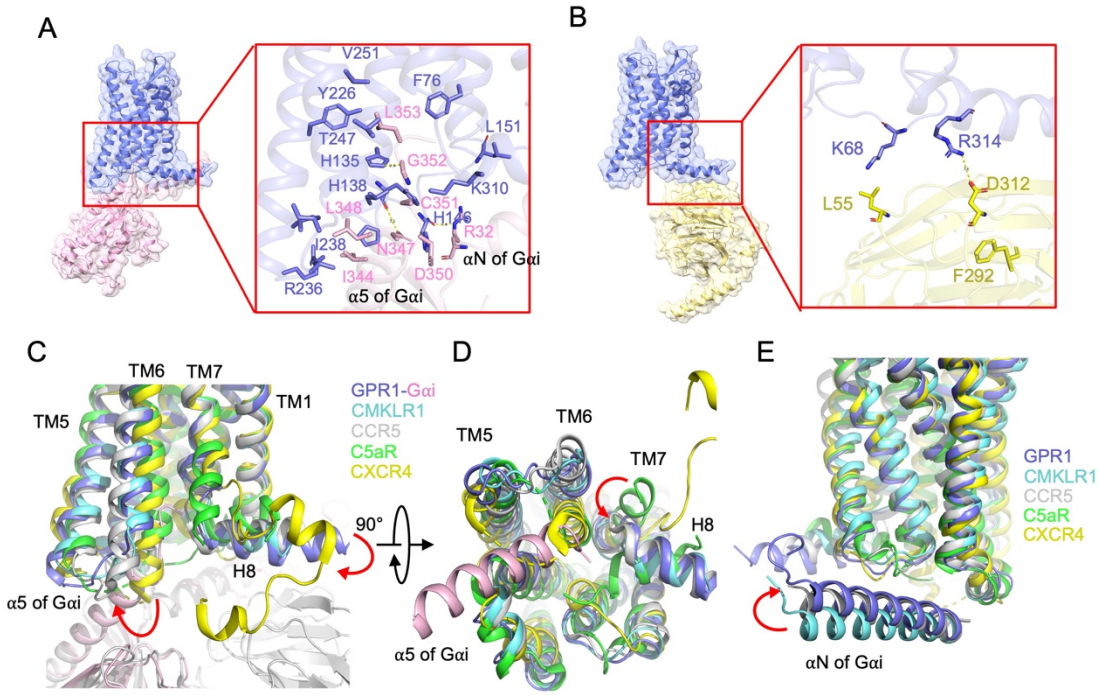

Figure 6. G protein interface of the C9-bound GPR1-Gi complex. (A) The interactions between the α5 helix of Gαi (pink) and GPR1 (marine blue) in the cavity at ICL3, TM5, TM6, and TM7 regions. **(B)** The interactions between Gβ subunit (yellow) and H8 of the receptor (marine blue). **(C)** Comparisons of the interactions between the α5 helix of Gαi and TM5, TM6, and ICL3 of several Gi-coupled receptors including GPR1 (marine blue), CMKLR1 (cyan, PDB ID: 7YKD), CCR5 (gray, PDB ID: 7F1R), C5aR (lime green, PDB ID: 6C1R) and CXCR4 (yellow, PDB ID: 3ODU). **(D)** 90°orientation of (C) for intracellular view showing the locations of ICL2, ICL1, and H8. **(E)** Same as (C) and (D) yet the interactions of the αN helix of Gαi with these receptors are compared.

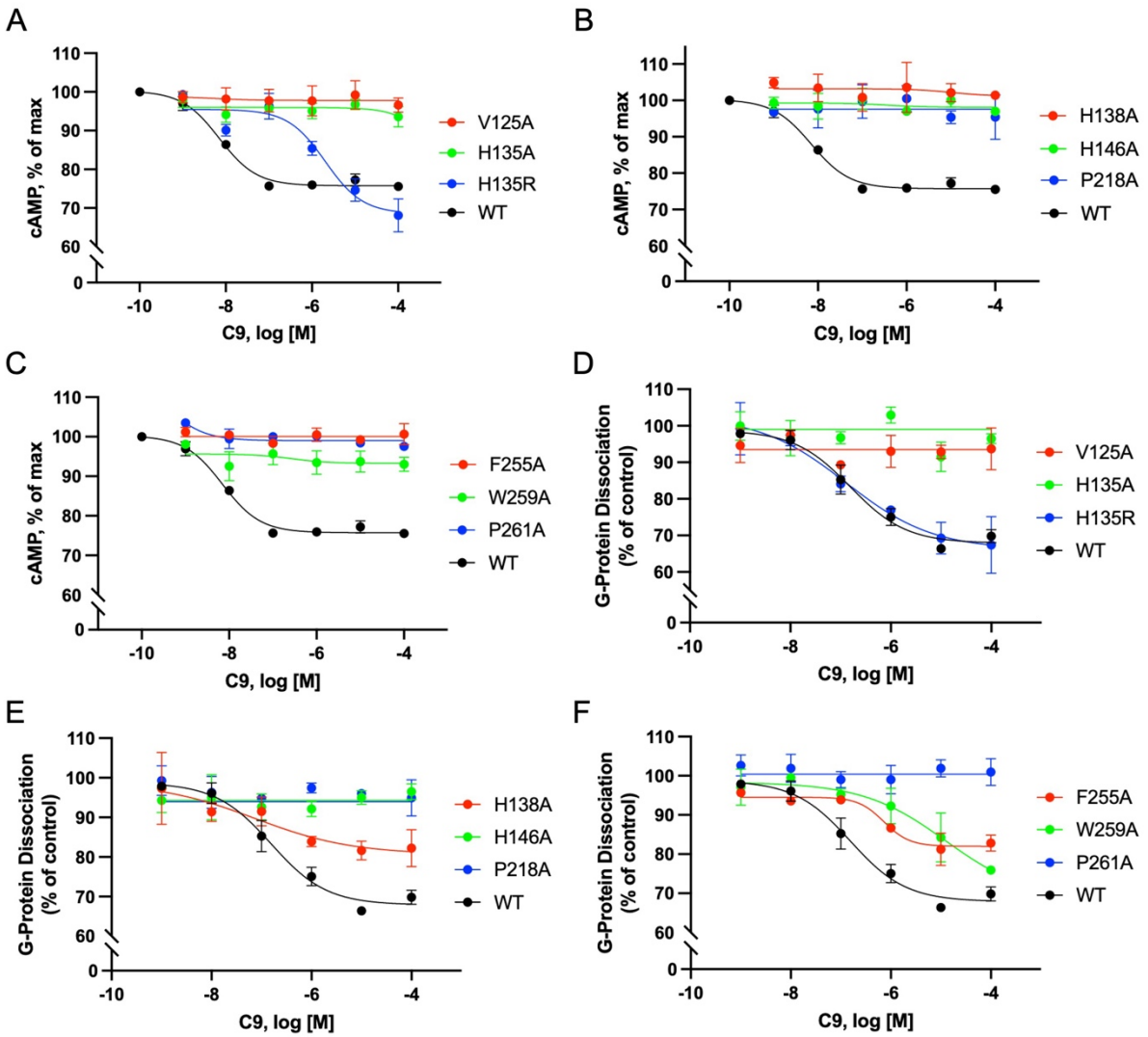

Figure 7. Point mutations at key residues for G protein activation affect cAMP inhibition and G protein dissociation. (A - C) cAMP response in HeLa cells transfected to express WT or mutant GPR1. Different concentrations of C9 are applied. **(D - F)** G protein dissociation in HEK293T cells co-transfected to express WT or mutant GPR1, Gαi1-LgBiT, Gβ1, and SmBiT-Gγ2. Different concentrations of C9 are applied. All data shown are means ± SEM from three independent experiments.